The LH-DH module of the bacterial replicative helicases is the common binding site for DciA and other helicase loaders

Claire Cargemel, Stéphanie Marsin, Magali Noiray, Pierre Legrand, Halil Bounoua, Inès Li de la Sierra-Gallay, Hélène Walbott, Sophie Quevillon-Cheruel

The LH-DH module of the bacterial replicative helicases is the common binding site for DciA and other helicase loaders

Claire Cargemel[1], Stéphanie Marsin[1], Magali Noiray[1], Pierre Legrand[2], Halil Bounoua[1], Inès Li de la Sierra-Gallay[1], Hélène Walbott[1¶], Sophie Quevillon-Cheruel[1¶]

[1] Université Paris-Saclay, CEA, CNRS, Institute for Integrative Biology of the Cell (I2BC), 91198, Gif-sur-Yvette, France.

[2] Synchrotron SOLEIL, L'Orme des Merisiers, 91192 Gif-sur-Yvette, France.

[¶] Correspondence: helene.walbott@i2bc.paris-saclay.fr and sophie.quevillon-cheruel@i2bc.paris-saclay.fr

RUNNING TITLE

Crystal structure of DnaB•DciA complex

KEYWORDS

DnaB•DciA complex / structural study / Interaction module / replicative helicase hijacking

Abstract

During the initiation step of bacterial genome replication, replicative helicases depend on specialized proteins for their loading onto *oriC*. DnaC and DnaI were the first loaders characterized. However, most bacteria do not contain any of these genes, which are domesticated phage elements that replaced the ancestral and unrelated loader gene *dciA* several times during evolution. To understand how DciA assists the loading of DnaB, we determined the crystal structure of the complex from *Vibrio cholerae*, in which two *Vc*DciAs interact with a dimer of *Vc*DnaB, without changing its canonical structure. Our data showed that the *Vc*DciA binding site on *Vc*DnaB is the conserved module formed by the linker helix LH of one monomer and the determinant helix DH of the second one. Interestingly, DnaC from *Escherichia coli* also targets this module onto *Ec*DnaB. Thanks to their common target site, we showed that *Vc*DciA and *Ec*DnaC could be functionally interchanged *in vitro*, despite sharing no structural similarities. This is a milestone in understanding the mechanism employed by phage helicase loaders to hijack bacterial replicative helicases during evolution.

Introduction

The replication of the circular bacterial chromosome is an essential step for bacterial division. The initiator protein DnaA initiates the replication by binding onto the origin DNA *oriC*, and unwinds locally the double-strand DNA by polymerization (Costa, Hood et al., 2013, Leonard & Méchali, 2013, Zawilak-Pawlik, Nowaczyk et al., 2017). Then, the toroidal hexameric helicase DnaB is loaded onto the locally open DNA duplex, with the help of a helicase loader, triggering the recruitment of the various proteins of the replisome (O'Donnell, Langston et al., 2013). ATP-dependent 5′ to 3′ translocation of the helicase ahead of the advancing replisome allows unwinding DNA duplex into templates for new DNA synthesis (Strycharska, Arias-Palomo et al., 2013).

Recruitment and loading of the replicative helicase depend on a loader protein, which was characterized in the two model organisms *Escherichia coli* (*Ec*) and *Bacillus subtilis* (*Bs*), leading to the description of two loading strategies. In *Bacillus subtilis*, the helicase loader DnaI assists the assembly of six monomers of the helicase to form an active hexameric ring around DNA according to a "ring-maker" scenario (Davey & O'Donnell, 2003, Velten, McGovern et al., 2003). The *Gst*DnaB•*Bs*DnaI•*Gst*DnaG prepriming complex exhibits a three-layered planar and dilated ring conformation with one hexameric helicase binding to three loader protein dimers and three primase proteins (Liu, Eliason et al., 2013). In the *Escherichia coli* system, the helicase loader DnaC mediates the opening of the DnaB hexamer into a loading-competent cracked-open ring according to a "ring-breaker" scenario (Arias-Palomo, Puri et al., 2019, Nagata, Okada et al., 2020). The *Ec*DnaB•*Ec*DnaC complex is dodecameric with six subunits of each protein and the complex assembles into a three-tier spiral. *Ec*DnaC makes *Ec*DnaB contacts through the first small α-helix (15 residues long) of its extended N-terminal domain (NTD). This helix interacts with the DnaB module composed of the "linker helix" (LH) of one DnaB protomer and of an antiparallel α-helix of the adjacent DnaB protomer, which we named "determinant helix" (DH) in a previous study (Marsin, Adam et al., 2021), and was named "docking helix" in a recent review comparing the convergent functional mechanisms of *Ec*DnaC and bacteriophage λ P loaders (Chase, Berger et al., 2022). This forms a three α-helix bundle, which fixes the relative orientation of the two adjacent DnaB C-terminal domains (CTDs): the 6 DnaC thus latched onto the DnaB hexamer adopt a spiral configuration that causes a distortion in the helicase ring, resulting in its large opening as a means to allow single-strand DNA (ssDNA) to enter the helicase pore (Arias-Palomo et al., 2019, Nagata et al., 2020).

Yet, the DnaC/I loader distribution is marginal in the bacterial domain. It was established phylogenetically that *dnaC/I* genes are domesticated phage elements that replaced

several times through the evolution, the ancestral bacterial gene *dciA* (Brézellec, Vallet-Gely et al., 2016). DciA and DnaC/I are not related by either their sequence or their structure (Marsin et al., 2021). While the DnaC/I CTD contains an AAA+ ATPase RecA-like domain (Koonin, 1992), the DciA NTD folds as a KH domain (Grishin, 2001, Marsin et al., 2021) also shared by the domain I of DnaA and the domain V of DnaX both described to interact with DnaB (Haroniti, Anderson et al., 2004, Jameson, Rostami et al., 2014, Mary Rajathei & Selvaraj, 2013). Through multiple complementary approaches, we previously established that the disordered CTD of DciA can form transiently small helical structures (Chan-Yao-Chong, Marsin et al., 2020) and is necessary for interacting with DnaB and stimulating DnaB loading onto DNA (Chan-Yao-Chong et al., 2020, Marsin et al., 2021). The direct interplay between the two proteins has also been demonstrated using the variation of intrinsic fluorescence of the conserved tryptophan residue located in the middle of the DH of DnaB, in the presence of DciA (Marsin et al., 2021). It was therefore suspected that DciA interacts with the helicase nearby the DH helix of its module.

To decipher the molecular interactions between DciA and DnaB, we solved the crystal structure of the DnaB•DciA complex from *Vibrio cholerae* (*Vc*) together with ADP and Mg^{2+}, forming a heterotetramer, composed of the canonical *Vc*DnaB dimer and of two molecules of *Vc*DciA. Interestingly, *Vc*DciA interacts with *Vc*DnaB through the LH-DH module, like *Ec*DnaC and the phage λ P helicase loader on *Ec*DnaB, suggesting a functional link between the different systems. Furthermore, we showed that *Vc*DciA and *Ec*DnaC are interchangeable for the *in vitro* loading of the helicases from *V. cholerae* and *E. coli*, demonstrating that the substitution of *dciA* by *dnaC* triggered only local adaptation during evolution. But the *Vc*DnaB•*Vc*DciA•ADP:Mg^{2+} structure also revealed that DciA binds to the periphery of the helicase CTD contrary to other known loaders that are positioned at the back of the DnaB

CTD ring, presuming that its helicase loading mechanism is different from those of DnaC/I and λ P.

Results and discussion

The crystal structure of the *Vc*DnaB•*Vc*DciA complex forms a heterotetramer with a 2:2 stoichiometry

We have previously demonstrated by functional studies that DciA from *Vibrio cholerae* (*Vc*) increases the loading of *Vc*DnaB on DNA, resulting in an increased unwinding activity of the helicase (Marsin et al., 2021). To understand the molecular interplay between the two proteins, we determined the crystal structure of the *Vc*DnaB•*Vc*DciA•ADP:Mg^{2+} complex (PDB ID 8A3V, this study). The structure was solved by molecular replacement (see Materials and Methods and Table 1) using the *Vc*DnaB•GDP:AlF_4:Mg^{2+} crystal structure (PDB ID 6T66) (Marsin et al., 2021), the *Vc*DciA$^{[1-111]}$ NMR structure (BMRB ID 27689) (Marsin et al., 2021) and the full-length *Vc*DciA model predicted by AlphaFold2 (Jumper, Evans et al., 2021), and refined to 2.9 Å resolution. The accuracy of the final model was further verified by superimposition on an experimental electron density map obtained at 3.7 Å resolution by single-wavelength anomalous diffraction (SAD) using derivative data from a $(Ta_6Br_{12})^{2+}$-cluster-soaked crystal (see Materials and Methods and Table 1).

The asymmetric unit of the crystal contains two molecules of *Vc*DnaB and two molecules of *Vc*DciA. The crystal structure of the *Vc*DnaB•*Vc*DciA complex revealed domain swapping between symmetry related molecules of *Vc*DciA (Figure 1A). The NTD and CTD (N-terminal and C-terminal domains) of the two *Vc*DciA connected by an extended hinge region (residues E99 to S121) are exchanged between neighboring molecules related by a true crystallographic 2-fold rotation axis. It is not known at present whether this domain swapping is due to a crystal artifact or whether it is biologically relevant. However, it is known that

replication is bidirectional and therefore two helicases must be recruited to the replication fork (Chodavarapu & Kaguni, 2016, Hayashi, Miyazaki et al., 2020). The ability of DciA to link helicases together via this domain swapping could therefore improve the recruitment of helicases to *oriC* and thus optimize the replication initiation step.

The *Vc*DnaB•*Vc*DciA heterotetramer structure can be reconstructed from the swapped domains between symmetric *Vc*DciAs (Figure 1B) and exhibits two *Vc*DciA fixed on a *Vc*DnaB dimer. The *Vc*DnaB dimer in the heterotetrameric complex is bound to ADP:Mg^{2+} and is almost identical to one *Vc*DnaB dimer of the GDP-bound *Vc*DnaB hexamer structure (PDB ID 6T66 (Marsin et al., 2021)), with an overall RMSD of 1.76 Å (RMSD of 0.99 Å for the NTDs and 1.26 Å for the CTDs) (Figure supplement 1A). The NTP:Mg^{2+} binding site into the CTDs is very similar, the P-loop is in the same conformation (Figure supplement 1B). Therefore, the formation of the complex with *Vc*DciA does not alter the overall canonical architecture of the *Vc*DnaB dimer nor the NTP binding site. Nevertheless, the binding of *Vc*DciA on the LH-DH module of *Vc*DnaB slightly accentuates the gap between the LH and DH helices of about 5 Å, relatively to the module in the free *Vc*DnaB hexamer structure (Figure supplement 1A). The two *Vc*DciA of the heterotetrameric complex are practically identical to each other (RMSD of 0.48 Å for the NTDs and 0.20 Å for the CTDs), except for the first long α1 helix which is straight in the first *Vc*DciA molecule and kinked with an angle of 50° at residue H24 in the second one (Figure supplement 1C). This kink can be explained because of a steric hindrance with the extended hinge of the neighboring symmetric *Vc*DciA molecule with which they are engaged in domain swapping. This possibility of bending the long α1 helix of *Vc*DciA was predicted by our previous molecular dynamics analyses (Chan-Yao-Chong et al., 2020). The NTD domain of *Vc*DciA in this crystal structure exhibits a KH-like fold very similar to the *Vc*DciA$^{[1\text{-}111]}$ structure (BMRB 27689 (Marsin et al., 2021)) we obtained by NMR (RMSD of 1.28 Å, Figure supplement 1C). However, the CTD tail of

150 *Vc*DciA, observed as disordered in solution by SAXS (Marsin et al., 2021), folds into a small
151 helix hairpin in contact with *Vc*DnaB (Figure supplement 1D), again in agreement with our
152 previous molecular dynamics analyses (Chan-Yao-Chong et al., 2020). The structure of the
153 extended hinge region consisting of the last helix of the NTD and the proline-rich flexible
154 linker, which connects the NTD to the CTD of *Vc*DciA, is only putative in this model,
155 reconstructed from the swapped domains.

156 The two *Vc*DciA molecules interact "*in trans*" with the *Vc*DnaB dimer at the periphery
157 of the CTDs (Figure 1B). The CTD hairpin helix of one *Vc*DciA molecule stacks entirely on
158 the LH-DH module of *Vc*DnaB (in magenta in Figure 1C). The kinked α2 helix of the NTD of
159 the second *Vc*DciA (in yellow in Figure 1C) interacts with the first helix of the CTD hairpin
160 of the first *Vc*DciA (approximately 238.0 $Å^2$ of "*in trans*" interaction interface between the
161 CTD and NTD from two different *Vc*DciAs, as measured by PDBePISA server (Krissinel &
162 Henrick, 2007)) and also with the DH helix of *Vc*DnaB. The assembly forms a 5-helix bundle
163 (Figure 1C). In addition to the kinked α2 helix, the β3 strand of the *Vc*DciA NTD also
164 interacts at the periphery of the *Vc*DnaB CTD, particularly with the DH helix. This DH helix
165 (determinant/docking helix) is thus at the heart of the interaction between *Vc*DciA and
166 *Vc*DnaB, as proposed by our previous Tycho experiments (Marsin et al., 2021). The overall
167 interaction interface of a *Vc*DciA molecule with a *Vc*DnaB dimer is about 1264.4 $Å^2$, with
168 about 514.8 $Å^2$ for the NTD of *Vc*DciA and about 749.6 $Å^2$ for its CTD (from PDBePISA
169 server (Krissinel & Henrick, 2007)). The structure of the complex therefore confirmed the
170 essential role played by the CTD of *Vc*DciA in the interaction with *Vc*DnaB as shown by our
171 previous ITC experiments (Chan-Yao-Chong et al., 2020). Finally, it should be noted that the
172 NTD of the *Vc*DciA molecule with a kinked α1 helix is less well-defined in the density, which
173 can be explained by the fact that its interaction interface with the CTD of *Vc*DnaB is only
174 about 346.9 $Å^2$ versus 514.8 $Å^2$ for the *Vc*DciA NTD with a straight α1 helix. This binding

175 difference between the NTDs of the two *Vc*DciAs is likely caused by different steric
176 constraints due to crystal packing and/or related to domain swapping.
177
178 **Both *Vc*DciA and *Ec*DnaC loaders target the conserved LH-DH module of DnaB**
179 **helicases and are functionally interchangeable *in vitro***
180 The LH-DH module is conserved in DnaB helicases (Chase et al., 2022). However, we have
181 previously identified a residue in the DH helix that discriminates DciA helicases from DnaC/I
182 helicases (respectively a serine and a glycine) (Marsin et al., 2021) (Figure 2A). Moreover,
183 the *Vc*DciA and *Ec*DnaC loaders have no sequence or structural similarity. Yet, the two
184 loaders target the same binding site on the helicase: the conserved LH-DH module of DnaB,
185 although the interaction interfaces are quite different (Figure 2B). This interaction involves a
186 single small α-helix of the NTD end of *Ec*DnaC, forming a 3-helix bundle, whereas in
187 *Vc*DciA, the CTD helix hairpin and the elbow of the kinked α2 helix of NTD participate both
188 in, forming a 5-helix bundle. We can wonder at this stage if this common target on DnaB, the
189 LH-DH module, allows a cross-talk between the two helicase-loader systems, despite the
190 specificities of each of them.
191 Using Tycho nano-DSF technology, the fluorescence variation of tryptophan residues
192 can be followed in real time along thermal ramp (see Materials and Methods). Ideally, a
193 conserved tryptophan is located in the DH helix, namely W291 for *Vc*DnaB and W294 for
194 *Ec*DnaB (Figures 2A and 2B) (Marsin et al., 2021). A second conserved tryptophan is located
195 in the globular head of the NTD domain of DnaB (positions 45 and 48 in *Vc*DnaB and
196 *Ec*DnaB, respectively), but is buried and cannot participate in any protein-protein interactions.
197 *Vc*DciA does not contain any tryptophan in its sequence. We previously demonstrated the
198 binding of *Vc*DciA in proximity of the LH-DH module of *Vc*DnaB using this technology
199 (Marsin et al., 2021), showing that W291 is inaccessible to solvent when *Vc*DnaB interacts

with *Vc*DciA. We further showed that *Vc*DciA deleted from its CTD (*Vc*DciA$^{[1\text{-}111]}$) can no longer bind *Vc*DnaB (Figure 2C left), as expected if the CTD of *Vc*DciA covers the DH α-helix of *Vc*DnaB (Figure 2B). On the other hand, *Ec*DnaB contains a third non-conserved tryptophan residue, solvent-exposed in its CTD. *Ec*DnaC also encloses three solvent-exposed tryptophan residues in its sequence, one in its NTD extended end (W32 in Figure 2B) and two in its CTD. All these tryptophan residues could therefore participate in protein-protein interactions. Indeed, Tycho allowed to confirm the interaction between *Ec*DnaB and *Ec*DnaC by comparing the lower initial 350 nm / 330 nm ratio for the measured curve (in red, Figure 2D left) than for the theoretical curve representing the absence of solvent protection (in black, Figure 2D left). In addition, *Ec*DnaC deleted from its NTD (*Ec*DnaC$^{[53\text{-}end]}$) can no longer bind *Ec*DnaB (Figure 2D left), as expected if the α1 helix of *Ec*DnaC forms a 3-helix bundle with the LH-DH module of *Ec*DnaB (Figure 2B). These findings are in agreement with the 3D structures of the two complexes: the interaction takes place at the DH of DnaB and requires the CTD for DciA and the NTD for DnaC. We further carried out crossover experiments with the heterologous *Vc*DnaB/*Ec*DnaC and *Ec*DnaB/*Vc*DciA systems. We showed efficient non-cognate helicase-loader interactions, which also require the NTD of *Ec*DnaC (Figure 2C right) and the CTD of *Vc*DciA (Figure 2D right).

We then investigated if these interactions are relevant for the stimulation of the helicase loading on DNA by the loaders. We attached a 3'-biotinylated 50-mer ssDNA to a streptavidin-coated probe to measure interactions using the bio-layer interferometry (BLI, see Materials and Methods). We monitored in real-time interactions between immobilized ssDNA and the helicases in the presence of different concentrations of loaders (Figure 3). The BLI experiments confirmed the results already observed by SPR (Marsin et al., 2021), namely that the loading stimulation of both helicases increases with the concentration of added cognate loader, *Vc*DciA or *Ec*DnaC (Figures 3A and 3B left), at concentrations for which the response

for loaders alone is negligible (Figure supplement 2). Moreover, on the same conditions, *Ec*DnaC is able to load *Vc*DnaB onto the ssDNA, and *Vc*DciA to load *Ec*DnaB (Figures 3A and 3B right). The cross-talk is effective *in vitro*, there seems to be a functional convergence between the two systems. *Ec*DnaB apparently had little need to evolve to accommodate DnaC, after DciA was replaced. This could explain why the replacement of DciA by DnaC/I occurred at least 7 times during evolution, and how phage loaders were able to hijack bacterial replicative helicases efficiently (Brézellec et al., 2016).

_Vc_DciA binds to the periphery of the _Vc_DnaB CTD, in contrast to other loaders, which are positioned at the back of the helicase CTD ring

Our previous SEC-SAXS and SEC-MALS experiments showed that a complex between the *Vc*DnaB hexamer and *Vc*DciA is formed in solution *in vitro* but is not stable and tends to dissociate, which did not allow us to determine the precise stoichiometry of this complex (Marsin et al., 2021). Interestingly, the *H*32 symmetry of the crystal reconstitutes the heterododecamer complex by the assembly of the heterotetramer with two neighboring symmetry mates related by a true crystallographic 3-fold rotation axis (Figure 4A). Further work remains to be done to find out if this heterododecameric structure is biologically relevant or not, but in the meantime, we can compare it with other helicase-loader structures in the literature. Three 3D structures of helicase-loader complexes are currently known: *Ec*DnaB•*Ec*DnaC (PDB ID 6QEL (Arias-Palomo et al., 2019)), *Ec*DnaB•λP (PDB ID 6BBM (Chase, Catalano et al., 2018)) and *Gst*DnaB•*Bs*DnaI (PDB ID 4M4W (Liu et al., 2013)). Strikingly, *Vc*DciA binds to the periphery of the *Vc*DnaB CTD, in contrast to the other three loaders, which are positioned at the back of the helicase CTD ring (Figure 4B). The loading mechanism used by DciA has still to be elucidated but we can assume that it will probably be different from those already described for the other three loaders.

Concluding remarks

The two genes coding for DciA and DnaC/I are unrelated and mutually exclusive in the bacterial genomes (Brézellec, Petit et al., 2017, Brézellec et al., 2016). However, like DnaC and the bacteriophage λ P helicase loader (Arias-Palomo et al., 2019, Chase et al., 2022, Chase et al., 2018), DciA interacts with the two-helix LH-DH module of DnaB. This "binding module", conserved in the bacterial replicative helicases, suggests a functional link between the different systems. Moreover, *Ec*DnaB, although likely to have evolved to accommodate the replacement of DciA by DnaC during evolution, retains the ability to be loaded by both loaders *in vitro*. Nevertheless, the structural data on the *Vc*DnaB•*Vc*DciA•ADP:Mg^{2+} complex provided here permit us to postulate that DciA is probably not a helicase loader of the "ring-maker" or the "ring-breaker" types, strictly speaking, and that its action boosts the loading of the replicative helicase through a new mechanism that remains to be elucidated.

Materials and methods

Protein samples preparation

*Vc*DnaB, *Ec*DnaB, *Vc*DciA, *Vc*DciA$^{[1\text{-}111]}$ and *Ec*DnaC were overexpressed in *E. coli* and purified as described in (Marsin et al., 2021). *Ec*DnaC$^{[53\text{-}end]}$ was purified as *Ec*DnaC. Strains and plasmids are available upon request.

Crystal structure determination of the *Vc*DnaB•*Vc*DciA•ADP:Mg^{2+} complex

Purified *Vc*DnaB was preincubated for 10 min at 4°C at a concentration of 0.115 mM (monomer) with 2 mM ADP + 5 mM $MgCl_2$. Purified *Vc*DciA was added at a final concentration of 0.138 mM (about 7 monomers of DciA per helicase hexamer) for a second step of incubation. Native protein crystals were grown in sitting drops by mixing the proteins

with the reservoir solution in a 1:1 ratio. Rhombohedral crystals of the *Vc*DnaB•*Vc*DciA•ADP:Mg^{2+} complex appeared after 5 days at 18°C in 0.1 M sodium acetate (pH 4.8 - 5.6) + 0.7 to 0.9 M potassium/sodium tartrate. For derivatization, single crystals were then soaked for 2 hours at 18°C in a solution containing 1 mM $(Ta_6Br_{12})^{2+}$ cluster (JBS Tantalum Cluster Derivatization Kit from Jena Bioscience GmbH, Jena, Germany). 25% glycerol cryo-protected native crystals or 50/50 paratone/paraffin oil mixture cryo-protected derivative crystals were flash-frozen in liquid nitrogen.

Diffraction data collection, phasing and refinement statistics are given in Table 1. Native and derivative crystallographic data were collected on the PROXIMA-2A and PROXIMA-1 beamlines, respectively, at the SOLEIL Synchrotron (Saint-Aubin, France) and processed with XDS (Kabsch, 2010) through XDSME (https://github.com/legrandp/xdsme) (Legrand, 2017). The strong diffraction anisotropy was corrected using the STARANISO server (http://staraniso.globalphasing.org) (Tickle, 2018). The *Vc*DnaB•*Vc*DciA•ADP:Mg^{2+} complex crystal structure was solved by molecular replacement (MR) with the MOLREP program (Vagin & Teplyakov, 2010) using the X-ray structures of the NTD [22-175] and CTD [200-461] isolated domains of *Vc*DnaB•GDP:AlF_4:Mg^{2+} as search models (PDB ID 6T66 (Marsin et al., 2021)). Two copies of each domain were correctly positioned. The initial model was then manually corrected and completed using COOT (Emsley, Lohkamp et al., 2010). Significant extra electron density allowed the manual building of the CTD isolated domains of two *Vc*DciA monomers, whose chains could be assigned using the 3D model of the full-length *Vc*DciA predicted by AlphaFold2 (Jumper et al., 2021) through the ColabFold server (Mirdita, Schütze et al., 2022). Additional electron density allowed the manual positioning of the NTD isolated domains of two *Vc*DciA monomers, using the NMR structure of *Vc*DciA$^{[1\text{-}111]}$ solved in (Marsin et al., 2021) (BMRB ID 27689). Finally, manual building of the linker regions connecting the NTD and CTD domains of *Vc*DciA revealed domain

swapping between symmetry related molecules of *Vc*DciA. The *Vc*DnaB•*Vc*DciA•ADP:Mg^{2+} complex structure was iteratively improved by manual building steps followed by refinement cycles using native data to 2.9 Å resolution. The model refinement was conducted with the BUSTER program (Bricogne, Blanc et al., 2017) using 12 translation–libration–screw (TLS) motion groups, automated non-crystallographic symmetry (NCS) restraints and local structure similarity restraints (LSSR) to the target models of the *Vc*DnaB•*Vc*DciA complex predicted by AlphaFold2 (Jumper et al., 2021, Mirdita et al., 2022) mirand RoseTTAFold (Baek, DiMaio et al., 2021).

To avoid model bias, an experimental electron density map was obtained at 3.7 Å resolution by single-wavelength anomalous diffraction (SAD) using derivative data collected at the tantalum (Ta) peak wavelength. The $(Ta_6Br_{12})^{2+}$ cluster sites were initially found with SHELXD (Schneider & Sheldrick, 2002), then phases were determined with PHASER (McCoy, Grosse-Kunstleve et al., 2007) and improved by density modification with the PARROT program (Cowtan, 2010) through the CCP4 software suite (Winn, Ballard et al., 2011). Superimposing the MR model on the experimental map confirmed its accuracy, except for the NTD of the second *Vc*DciA monomer for which no density was visible, likely due to a too sharp solvent flattening. Crystals of *Vc*DnaB•*Vc*DciA•ADP:Mg^{2+} complex were analyzed by SDS-PAGE and both *Vc*DnaB and *Vc*DciA were visualized on the gel after Coomassie Blue staining as full-length proteins without any proteolysis (Figure supplement 3). The BUSTER program (Bricogne et al., 2017) calculated per-residue values for real-space correlation of the final refined model against the 2fo-fc map. The NTD of the second *Vc*DciA molecule has an acceptable mean real-space correlation coefficient (RSCC) of about 0.7, although a bit lower than the mean RSCC of about 0.8 of the NTD of the first *Vc*DciA which is very similar to the overall average RSCC of the whole model. This reflects a difference in

flexibility between the NTDs of the 2 *Vc*DciA monomers, likely due to crystal packing and domain swapping constraints.

All structural figures were prepared using PyMOL software (https://pymol.org) (DeLano, 2002).

Protein interaction analysis by thermal shift assay and intrinsic fluorescence variation

As described in (Marsin et al., 2021), intrinsic fluorescence changes of tryptophan (and tyrosine at a lower level) are recorded at 330 and 350 nm while heating the protein sample from 35 to 95°C at a rate of 3°C/min. The emission profile of tryptophan is shifted to the red emissions when it is released to the solvent during the thermal denaturing of the protein. We used Tycho analysis (Tycho NT.6, NanoTemper Technologies GmbH, Munich, Germany) to follow the interaction between *Vc*DnaB or *Ec*DnaB and *Vc*DciA, *Vc*DciA$^{[1\text{-}111]}$, *Ec*DnaC or *Ec*DnaC$^{[53\text{-}end]}$. Interactions were performed in Hepes 50 mM at pH7.5, NaCl 150 mM, ATP 1 mM, with 20 µM of each protein, in capillary tubes of 10 µl. Three to five replicates were obtained to increase results confidence. To detect binding, we compared the 350/330 nm ratio of fluorescence of the complex with the predicted ratio we should obtain in absence of interaction (S brightness at 350 nm / S brightness at 330 nm).

Measurement of protein-DNA interaction by bio-layer interferometry (BLI)

BLI experiments were conducted using a Pall ForteBio's Octet® RED96e system (Fremont, CA, USA), using Streptavidin (SA) Biosensors. BLI monitors wavelength shifts (nm) resulting from changes in the optical thickness of the sensor surface during association or dissociation of the analyte. All BLI experiments were performed at 30℃ under 1000 rpm

stirring. The streptavidin biosensor was hydrated in a 96-well plate containing PBS buffer (Biorad) for at least 10 min before each experiment. 3' biotinylated oligonucleotide oso13 (50 nt long ssDNA, at 10 nM) (Biotin-GCAGGCTCGTTACGTAGCTGTACCG$(dT)_{25}$) was immobilized in PBS onto the surface of the SA biosensor through a cycle of Baseline (120 s), Loading (300 s), and Baseline (120 s). Association interactions were then monitored during 300 seconds in wells containing 200 µL samples at 100 nM of *Vc*DnaB or *Ec*DnaB with different ratios of the indicated loader in buffer HNATM1 (50 mM Hepes pH7, 150 mM NaCl, 1 mM ATP, 0.1% Tween20, 1 mM $MgCl_2$). At the end of each binding step, the sensors were transferred into a protein-free binding buffer HNATM1 to follow the dissociation kinetics for 600 s. The sensors can be recycled by dipping in 0.08% SDS for 10 seconds. The experiments have been carried out in duplicate, only one is presented.

Data Availability

The PDB accession number for the crystal structure of the *Vc*DnaB•*Vc*DciA•ADP:Mg^{2+} complex reported in this paper is 8A3V.

Funding

This work was supported by the French Infrastructure for Integrated Structural Biology (FRISBI) ANR-10-INBS-05, by funds from the Centre National de la Recherche Scientifique (CNRS) and by grants of the Region Ile de France. C.C. was supported by a Ph.D. fellowship from the French Ministry of Education.

Acknowledgments

X-ray diffraction data were collected at the SOLEIL Synchrotron (Saint-Aubin, France; PROXIMA-2A and PROXIMA-1 beamlines). We thank the beamline staff for their assistance

and advice during data collection. This work has benefited from the expertise of the Macromolecular interactions measurements Platform and of the Crystallization Platform of I2BC (Gif-sur-Yvette, France), and we thank Magali Aumont-Nicaise and Stéphane Plancqueel respectively for their assistance. We are grateful to Dominique Durand for her ongoing support. We thank Jean-Luc Ferat for the initiating discussions.

Author Contributions

S.Q.-C. conceived this study; S.Q.-C. performed the cloning; C.C., H.B. and S.Q.-C. purified and crystallized the proteins; S.M. and M.N. performed the BLI and biochemical assays; H.W. and P.L. performed the X-ray structure determination and refinement with the contribution of I.L.S.-G.; H.W., S.M. and S.Q.-C. wrote the paper with input from all authors.

References

Arias-Palomo E, Puri N, O'Shea Murray VL, Yan Q, Berger JM (2019) Physical Basis for the Loading of a Bacterial Replicative Helicase onto DNA. *Molecular cell* 74: 173-184.e4

Baek M, DiMaio F, Anishchenko I, Dauparas J, Ovchinnikov S, Lee GR, Wang J, Cong Q, Kinch LN, Schaeffer RD, Millán C, Park H, Adams C, Glassman CR, DeGiovanni A, Pereira JH, Rodrigues AV, van Dijk AA, Ebrecht AC, Opperman DJ et al. (2021) Accurate prediction of protein structures and interactions using a three-track neural network. *Science (New York, NY)* 373: 871-876

Brézellec P, Petit MA, Pasek S, Vallet-Gely I, Possoz C, Ferat JL (2017) Domestication of Lambda Phage Genes into a Putative Third Type of Replicative Helicase Matchmaker. *Genome Biology and Evolution* 9: 1561-6

Brézellec P, Vallet-Gely I, Possoz C, Quevillon-Cheruel S, Ferat JL (2016) DciA is an ancestral replicative helicase operator essential for bacterial replication initiation. *Nature Communications* 7: 13271

Bricogne G, Blanc E, Brandl M, Flensburg C, Keller P, Paciorek W, Roversi P, Sharff A, Smart OS, Vonrhein C, Womack TO (2017) BUSTER version 2.1.3. . *Cambridge, United Kingdom: Global Phasing Ltd*

Chan-Yao-Chong M, Marsin S, Quevillon-Cheruel S, Durand D, Ha-Duong T (2020) Structural ensemble and biological activity of DciA intrinsically disordered region. *Journal of structural biology* 212: 107573

Chase J, Berger J, Jeruzalmi D (2022) Convergent evolution in two bacterial replicative helicase loaders. *Trends in biochemical sciences* 47: 620-630

Chase J, Catalano A, Noble AJ, Eng ET, Olinares PD, Molloy K, Pakotiprapha D, Samuels M, Chait B, des Georges A, Jeruzalmi D (2018) Mechanisms of opening and closing of the bacterial replicative helicase. *eLife* 7

Chodavarapu S, Kaguni J (2016) Replication Initiation in Bacteria. *Enzymes* 39: 1-30

Costa A, Hood IV, Berger JM (2013) Mechanisms for initiating cellular DNA replication. *Annual review of biochemistry* 82: 25-54

Cowtan K (2010) Recent developments in classical density modification. *Acta crystallographica Section D, Biological crystallography* 66: 470-8

Davey MJ, O'Donnell M (2003) Replicative helicase loaders: ring breakers and ring makers. *Current biology : CB* 13: R594-6

DeLano WL (2002) The PyMOL Molecular Graphics System. *DeLano Scientific, San Carlos, CA, USA*

Emsley P, Lohkamp B, Scott WG, Cowtan K (2010) Features and development of Coot. *Acta crystallographica Section D, Biological crystallography* 66: 486-501

Grishin NV (2001) KH domain: one motif, two folds. *Nucleic acids research* 29: 638-43

Haroniti A, Anderson C, Doddridge Z, Gardiner L, Roberts CJ, Allen S, Soultanas P (2004) The Clamp-loader–Helicase Interaction in Bacillus. Atomic Force Microscopy Reveals the Structural Organisation of the DnaB–τ Complex in Bacillus. *Journal of molecular biology* 336: 381-93

Hayashi C, Miyazaki E, Ozaki S, Abe Y, Katayama T (2020) DnaB helicase is recruited to the replication initiation complex via binding of DnaA domain I to the lateral surface of the DnaB N-terminal domain. *The Journal of biological chemistry* 295: 11131-43

Jameson KH, Rostami N, Fogg MJ, Turkenburg JP, Grahl A, Murray H, Wilkinson AJ (2014) Structure and interactions of the Bacillus subtilis sporulation inhibitor of DNA replication, SirA, with domain I of DnaA. *Molecular microbiology* 93: 975-91

Jumper J, Evans R, Pritzel A, Green T, Figurnov M, Ronneberger O, Tunyasuvunakool K, Bates R, Žídek A, Potapenko A, Bridgland A, Meyer C, Kohl SAA, Ballard AJ, Cowie A, Romera-Paredes B, Nikolov S, Jain R, Adler J, Back T et al. (2021) Highly accurate protein structure prediction with AlphaFold. *Nature* 596: 583-9

Kabsch W (2010) XDS. *Acta crystallographica Section D, Biological crystallography* 66: 125-32

Koonin EV (1992) DnaC protein contains a modified ATP-binding motif and belongs to a novel family of ATPases including also DnaA. *Nucleic acids research* 20: 1997

Krissinel E, Henrick K (2007) Inference of macromolecular assemblies from crystalline state. *Journal of molecular biology* 372: 774-97

Legrand P (2017) XDSME: XDS Made Easier *GitHub repository*

Leonard AC, Méchali M (2013) DNA replication origins. *Cold Spring Harbor perspectives in biology* 5: a010116

Liu B, Eliason WK, Steitz TA (2013) Structure of a helicase-helicase loader complex reveals insights into the mechanism of bacterial primosome assembly. *Nature Communications* 4: 2495

Marsin S, Adam Y, Cargemel C, Andreani J, Baconnais S, Legrand P, Li de la Sierra-Gallay I, Humbert A, Aumont-Nicaise M, Velours C, Ochsenbein F, Durand D, Le Cam E, Walbott H, Possoz C, Quevillon-Cheruel S, Ferat JL (2021) Study of the DnaB:DciA interplay reveals insights into the primary mode of loading of the bacterial replicative helicase. *Nucleic acids research* 49: 6569-6586

Mary Rajathei D, Selvaraj S (2013) Analysis of sequence repeats of proteins in the PDB. *Computational biology and chemistry* 47: 156-66

McCoy AJ, Grosse-Kunstleve RW, Adams PD, Winn MD, Storoni LC, Read RJ (2007) Phaser crystallographic software. *Journal of applied crystallography* 40: 658-674

Mirdita M, Schütze K, Moriwaki Y, Heo L, Ovchinnikov S, Steinegger M (2022) ColabFold: making protein folding accessible to all. *Nature methods* 19: 679-682

Nagata K, Okada A, Ohtsuka J, Ohkuri T, Akama Y, Sakiyama Y, Miyazaki E, Horita S, Katayama T, Ueda T, Tanokura M (2020) Crystal structure of the complex of the interaction domains of Escherichia coli DnaB helicase and DnaC helicase loader: structural basis implying a distortion-accumulation mechanism for the DnaB ring opening caused by DnaC binding. *Journal of biochemistry* 167: 1-14

O'Donnell M, Langston L, Stillman B (2013) Principles and concepts of DNA replication in bacteria, archaea, and eukarya. *Cold Spring Harbor perspectives in biology* 5

Robert X, Gouet P (2014) Deciphering key features in protein structures with the new ENDscript server. *Nucleic acids research* 42: W320-W324

Schneider TR, Sheldrick GM (2002) Substructure solution with SHELXD. *Acta crystallographica Section D, Biological crystallography* 58: 1772-9

Sievers F, Wilm A, Dineen D, Gibson TJ, Karplus K, Li W, Lopez R, McWilliam H, Remmert M, Söding J, Thompson JD, Higgins DG (2011) Fast, scalable generation of high-quality protein multiple sequence alignments using Clustal Omega. *Molecular systems biology* 7: 539

Strycharska MS, Arias-Palomo E, Lyubimov AY, Erzberger JP, O'Shea VL, Bustamante CJ, Berger JM (2013) Nucleotide and partner-protein control of bacterial replicative helicase structure and function. *Molecular cell* 52: 844-54

Tickle IJ, Flensburg, C., Keller, P., Paciorek, W., Sharff, A., Vonrhein, C., Bricogne, G. (2018) STARANISO. *Cambridge, United Kingdom: Global Phasing Ltd*

Vagin A, Teplyakov A (2010) Molecular replacement with MOLREP. *Acta crystallographica Section D, Biological crystallography* 66: 22-5

Velten M, McGovern S, Marsin S, Ehrlich SD, Noirot P, Polard P (2003) A two-protein strategy for the functional loading of a cellular replicative DNA helicase. *Molecular cell* 11: 1009-20

Winn MD, Ballard CC, Cowtan KD, Dodson EJ, Emsley P, Evans PR, Keegan RM, Krissinel EB, Leslie AG, McCoy A, McNicholas SJ, Murshudov GN, Pannu NS, Potterton EA, Powell HR, Read RJ, Vagin A, Wilson KS (2011) Overview of the CCP4 suite and current developments. *Acta crystallographica Section D, Biological crystallography* 67: 235-42

Zawilak-Pawlik A, Nowaczyk M, Zakrzewska-Czerwińska J (2017) The Role of the N-Terminal Domains of Bacterial Initiator DnaA in the Assembly and Regulation of the Bacterial Replication Initiation Complex. *Genes* 8

Figure Legends

Figure 1. Crystal structure of the *Vc*DnaB•*Vc*DciA•ADP:Mg^{2+} complex. **(A)** Domain-swapped heterooctamer. The crystal structure of the *Vc*$DnaB_2$•*Vc*$DciA_2$ complex revealed domain swapping between symmetry related molecules of *Vc*DciA. Left: Schematic representation of domain swapping. The NTD and CTD domains of the two *Vc*DciAs, connected by an extended hinge region (dark blue lines), are exchanged between neighboring molecules related by a true crystallographic 2-fold rotation axis (red dashed line). The four molecules of *Vc*DnaB are in two shades of blue and green, the four molecules of *Vc*DciA are in pink, purple, orange and brown. The four protein chains of the symmetry mate are marked with an apostrophe. Right: Ribbon representation of the heterooctameric structure, using the same colour code. **(B)** Structure of the *Vc*DnaB•*Vc*DciA•ADP:Mg^{2+} heterotetrameric complex

498 reconstituted from swapped domains. Left: Schematic representation. The hinges
499 encompassing residues 99-121 of the two *Vc*DciAs are putative in this model (dark blue
500 dotted lines). Right: Ribbon representation of the heterotetrameric structure. The *Vc*DnaB
501 dimer is in the same colours as in (A), the two *Vc*DciA molecules are in magenta and yellow.
502 The dark blue dotted rectangle frames the close-up view shown in (C). **(C)** Zoom-in on the
503 interface region forming a 5-helix bundle, with the superimposed experimental electron-
504 density map from SAD-phasing after solvent-flattening (gray mesh, contoured at 1σ).
505
506 **Figure 2.** *Vc*DciA and *Ec*DnaC target the same binding site on DnaB helicases. **(A)** Sequence
507 alignment of the LH and DH helices of *Vc*DnaB and *Ec*DnaB (generated by EMBL-EBI
508 Clustal Omega server (https://www.ebi.ac.uk/Tools/msa/clustalo/) (Sievers, Wilm et al.,
509 2011) and displayed using ESPript 3.0 server (https://espript.ibcp.fr) (Robert & Gouet, 2014).
510 The conserved residues are in white on a red background. An orange asterisk marks the
511 conserved tryptophans while a black one marks the specific serine/glycine residues in the DH
512 helix. **(B)** Close-up view of the interaction interface forming a three- or five-helix bundle
513 between the two-helix LH-DH module of DnaB (blue and green) and *Vc*DciA (top, in
514 magenta and yellow, PDB ID 8A3V, this study) or *Ec*DnaC NTD (bottom, in magenta, PDB
515 ID 6QEL), respectively. The tryptophans whose intrinsic fluorescence variation was measured
516 in the Tycho experiments are in orange sticks. **(C and D)** Tycho NT.6 analysis. The emission
517 profile of a tryptophan is shifted to the red emissions when it is released to the solvent during
518 the thermal denaturing of the protein. In red are reported the 350/330 nm ratios measured for
519 the different helicase-loader mixtures and in black are reported the predicted ratio in the
520 absence of interaction. The ratio comparisons are reported for each helicase-loader couple
521 indicated, namely for *Vc*DnaB (C) or *Ec*DnaB (D) with two constructs of *Vc*DciA or *Ec*DnaC.
522 The curves correspond to the mean ± SEM of three to five analyses. *Tycho interaction

523 analysis between *Vc*DnaB and *Vc*DciA was previously published (Marsin et al., 2021) but
524 nonetheless reproduced here for easiest evaluation with other helicase-loader couples.
525
526 **Figure 3.** *Vc*DciA and *Ec*DnaC loaders are functionally interchangeable *in vitro*. Bio-layer
527 interferometry (BLI) analysis using biotinylated oligonucleotide (50 nt) immobilized onto the
528 surface of a streptavidin (SA)-coated probe by its 3' extremity (see Materials and Methods).
529 Association was performed with the indicated helicase at a concentration of 100 nM during
530 300s in a buffer solution containing ATP and $MgCl_2$. Dissociation was assessed in the same
531 buffer for 600s. Increasing loader concentrations (from 0 to 200 nM in subunits, in blue to
532 red) were analyzed. The experiments were carried out in duplicate, only one is presented. **(A)**
533 *Vc*DnaB binding on ssDNA in the presence of *Vc*DciA (left) or *Ec*DnaC (right). **(B)** *Ec*DnaB
534 binding on ssDNA in the presence of *Ec*DnaC (left) or *Vc*DciA (right).
535
536 **Figure 4.** DciA binds to the periphery of the DnaB CTD. **(A)** Structure of the
537 *Vc*DnaB$_6$•*Vc*DciA$_6$ heterododecameric complex reconstituted by the crystal *H*32 symmetry.
538 The colour code is the same as in Fig 1B. Left: Schematic representation. The
539 heterododecameric ring is reconstituted by assembly of the heterotetramer with two
540 neighboring symmetry mates (hatching textures) related by a true crystallographic 3-fold
541 rotation axis (red dashed lines). The hinges encompassing residues 99-121 of the *Vc*DciA
542 molecules are putative in this model (dark blue dotted lines). Right: Ribbon representation of
543 the heterododecameric model. **(B)** Structural comparison of four helicase-loader complexes:
544 *Vc*DnaB•*Vc*DciA (PDB ID 8A3V, this study), *Ec*DnaB•*Ec*DnaC (PDB ID 6QEL),
545 *Ec*DnaB•λP (PDB ID 6BBM) and *Gst*DnaB•*Bs*DnaI (extracted from PDB ID 4M4W). The
546 DnaB hexamers are represented in surface (blue and green), and the helicase loaders in

magenta sticks. Unlike DnaC, λP and DnaI which cover the back of the DnaB CTD ring, DciA leaves it free by positioning itself at the periphery of the helicase.

Table 1. Data collection, phasing and refinement statistics

	Native	**$(Ta_6Br_{12})^{2+}$ derivative**
	***Vc*DnaB•*Vc*DciA•ADP:Mg^{2+} §**	***Vc*DnaB•*Vc*DciA•ADP:Mg^{2+} ‡**
Data collection		
Space group	*H*32	*H*32
Cell dimensions		
a, b, c (Å)	186.51, 186.51, 252.84	186.67, 186.67, 252.99
α, β, γ (°)	90.0, 90.0, 120.0	90.0, 90.0, 120.0
Wavelength (Å)	0.984	1.254
Resolution range (Å) †	48.3 – 2.9 (3.1 – 2.9)	49.8 – 3.7 (3.8 – 3.7)
Before STARANISO		
Measured/Unique reflections	651973/37637	423037/18409
Spherical completeness (%) †	99.9 (99.9)	99.1 (94.5)
Spherical anomalous completeness (%) †		98.6 (86.4)
$I/\sigma(I)$ †	7.9 (0.3)	6.0 (0.5)
After STARANISO		
Measured/Unique reflections	368086/21186	259130/11065
Ellipsoidal completeness (%) †	94.1 (71.7)	95.6 (97.0)
Ellipsoidal anomalous completeness (%) †		95.6 (94.7)
$I/\sigma(I)$ †	13.4 (1.6)	12.6 (2.0)
R_{merge} (%) †	19.6 (236.0)	22.3 (213.9)
R_{pim} (%) †	4.6 (54.1)	4.7 (45.6)
Redundancy †	17.4 (19.9)	23.4 (22.3)
Anomalous redundancy †		12.2 (11.6)
$CC_{1/2}$ †	0.999 (0.544)	0.999 (0.671)
CC_{ano} †		0.899 (0.0)
$\|DANO\|/\sigma(DANO)$		1.588 (0.767)
SAD phasing		
Number of sites		7
Overall FOM		0.311
Overall FOM after density modification		0.693
Refinement		
Resolution range (Å)	40.8 – 2.9	
Number of work/test reflections	20312/1229	
R/R_{free} (%)	29.8/30.8	
Geometry statistics		
Number of atoms	9367	
Protein	9311	
Ligand/ion	56	
Water	0	

R.m.s.d. from ideal values	
Bond lengths (Å)	0.005
Bond angles (°)	0.73
Average B-factor (Å^2)	
Overall	126.1
Protein	126.2
Ligand/ion	110.9
Ramachandran plot	
Most favoured (%)	96.4
Outliers (%)	0.5
Molprobity score	2.03

† Values in parentheses refer to the highest resolution shell.
§ Diffraction data collected from one crystal, which diffracted anisotropically to 2.88 Å along 0.894 *a** - 0.447 *b**, 2.88 Å along *b** and 5.21 Å along *c**.
‡ Diffraction data collected from one crystal, which diffracted anisotropically to 3.43 Å along 0.894 *a** - 0.447 *b**, 3.43 Å along *b** and 6.50 Å along *c**.

Additional Figure Legends

Figure supplement 1. Interaction with *Vc*DciA does not alter the overall structure of the *Vc*DnaB dimer but induces folding of the *Vc*DciA CTD into a helix hairpin. **(A)** Superimposition of the ADP-bound *Vc*DnaB dimer extracted from the complex with *Vc*DciA (cyan and green, PDB ID 8A3V, this study) with a GDP-bound *Vc*DnaB dimer extracted from the hexameric helicase ring (gray, PDB ID 6T66). The two structures of *Vc*DnaB are almost identical (global RMSD of 1.76 Å). However, the maximum distance between the LH and DH helices is increased by about 5 Å in the presence of *Vc*DciA (compare double red arrow with double orange arrow). **(B)** Zoom-in on the NTP binding site of the two superimposed *Vc*DnaB dimer structures (same colours as in (A)). The P-loops are perfectly superimposable, as well as the ADP (blue sticks) and the GDP-AlF_4 (gray sticks), and also the Mg^{2+} ions (cyan and gray spheres). **(C)** Superimposition of the two *Vc*DciA NTDs (yellow and magenta, PDB ID 8A3V, this study) extracted from the *Vc*DnaB•*Vc*DciA complex with the NMR structure of the isolated NTD of *Vc*DciA (in gray, BMRB ID 27689). The KH-like fold of the *Vc*DciA NTDs in the complex is very similar to the *Vc*DciA$^{[1\text{-}111]}$ NMR solution structure (RMSD of 1.28 Å). The two copies of *Vc*DciA NTD in the heterotetrameric structure are identical

579 (RMSD of 0.48 Å), except for the first long α1 helix (bend at residue H24 in one copy, with
580 an angle of 50° as illustrated by blue lines) and the last α3 helix (oriented almost oppositely in
581 the two copies with an angle of 135° as illustrated by blue lines). This reflects a certain
582 flexibility of *Vc*DciA which was predicted by previous molecular dynamics analyses (Marsin
583 et al., 2021). **(D)** Superimposition of the two *Vc*DciA CTDs (same colours as in (C)) extracted
584 from the complex with *Vc*DnaB. The *Vc*DciA CTD, which was shown disordered in solution
585 by SAXS (Marsin et al., 2021), folds into a helix hairpin upon interaction with the *Vc*DnaB
586 dimer (contact with the LH-DH module of the helicase). The two copies of *Vc*DciA CTD are
587 identical (RMSD of 0.20 Å).
588
589 **Figure supplement 2.** Interaction with ssDNA is detectable for neither *Vc*DciA nor *Ec*DnaC
590 under the same experimental conditions used for the helicase loading assays in this study. The
591 Bio-layer interferometry (BLI) analysis of the two loaders alone (from 0 to 200 nM in
592 subunits, in blue to red), is performed as described in Fig 3 and in the Materials and Methods
593 section.
594
595 **Figure supplement 3.** Validation of the protein composition of the *Vc*DnaB•*Vc*DciA complex
596 crystals. 11-month-old crystals of the complex were visualized by SDS-PAGE and Coomassie
597 Blue staining. Purified *Vc*DnaB and *Vc*DciA proteins were migrated on the same gel as
598 controls, showing that the crystallized proteins were protected from proteolysis. The crystals
599 of the complex obtained in our study grew in 5 days and were formed from the two full-length
600 proteins.

Fig 1

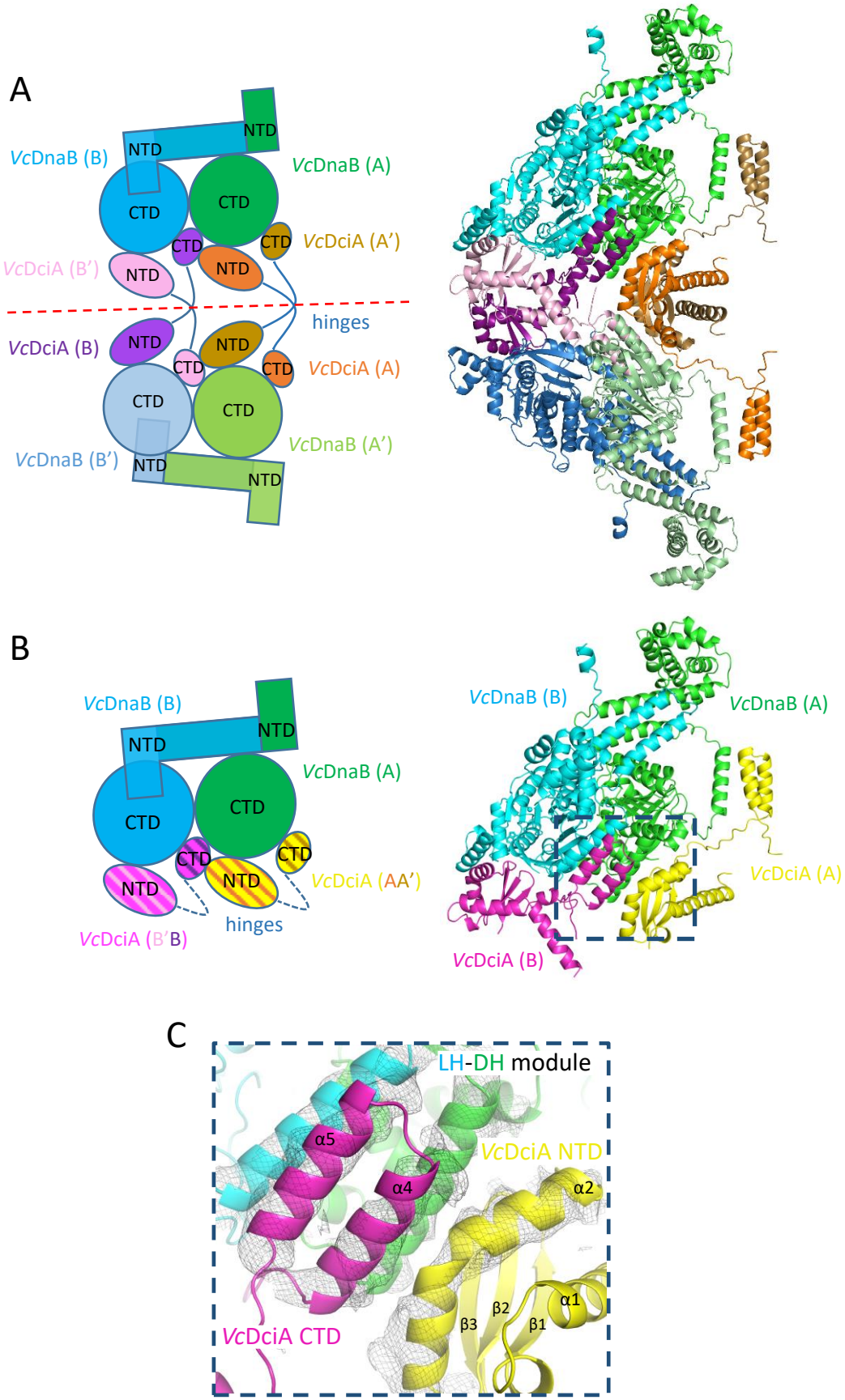
A
VcDnaB (B)
NTD
NTD
VcDnaB (A)
CTD
CTD
CTD
CTD
VcDciA (A')
VcDciA (B')
NTD
NTD
hinges
VcDciA (B)
NTD
NTD
CTD
CTD
VcDciA (A)
CTD
CTD
VcDnaB (A')
VcDnaB (B')
NTD
NTD
B
VcDnaB (B)
NTD
NTD
VcDnaB (A)
CTD
CTD
CTD
CTD
NTD
NTD
VcDciA (AA')
hinges
VcDciA (B'B)
VcDnaB (B)
VcDnaB (A)
VcDciA (A)
VcDciA (B)
C
LH-DH module
α5
VcDciA NTD
α4
α2
α1
β2
β3
β1
VcDciA CTD

Fig 2

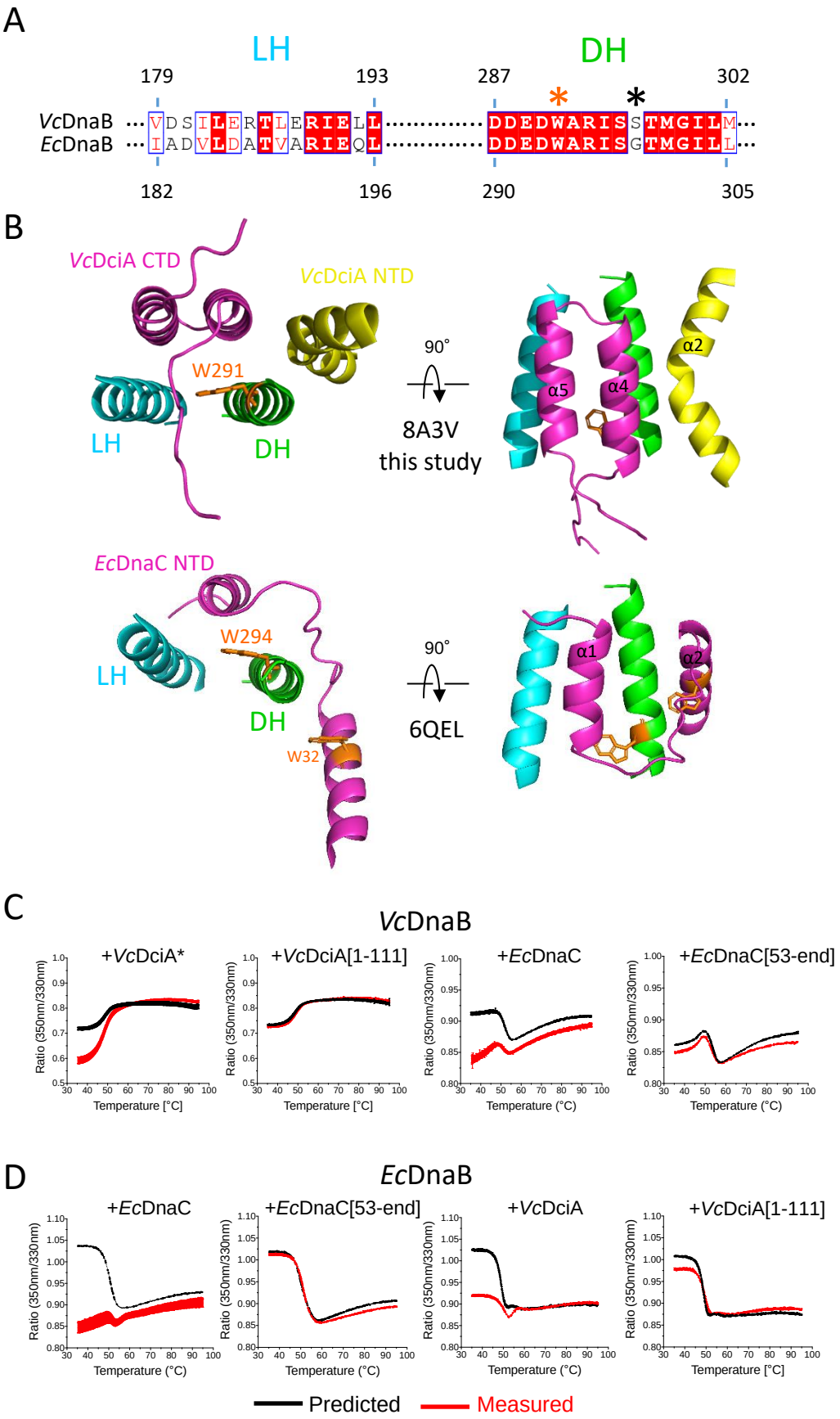
A
LH
DH
179
193
287
302
VcDnaB
EcDnaB
182
196
290
305
B
VcDciA CTD
VcDciA NTD
W291
LH
DH
90°
8A3V
this study
α2
α5
α4
EcDnaC NTD
W294
LH
DH
W32
90°
6QEL
α1
α2
C
VcDnaB
+VcDciA*
+VcDciA[1-111]
+EcDnaC
+EcDnaC[53-end]
Ratio (350nm/330nm)
Temperature [°C]
Temperature (°C)
D
EcDnaB
+EcDnaC
+EcDnaC[53-end]
+VcDciA
+VcDciA[1-111]
Predicted
Measured

Fig 3

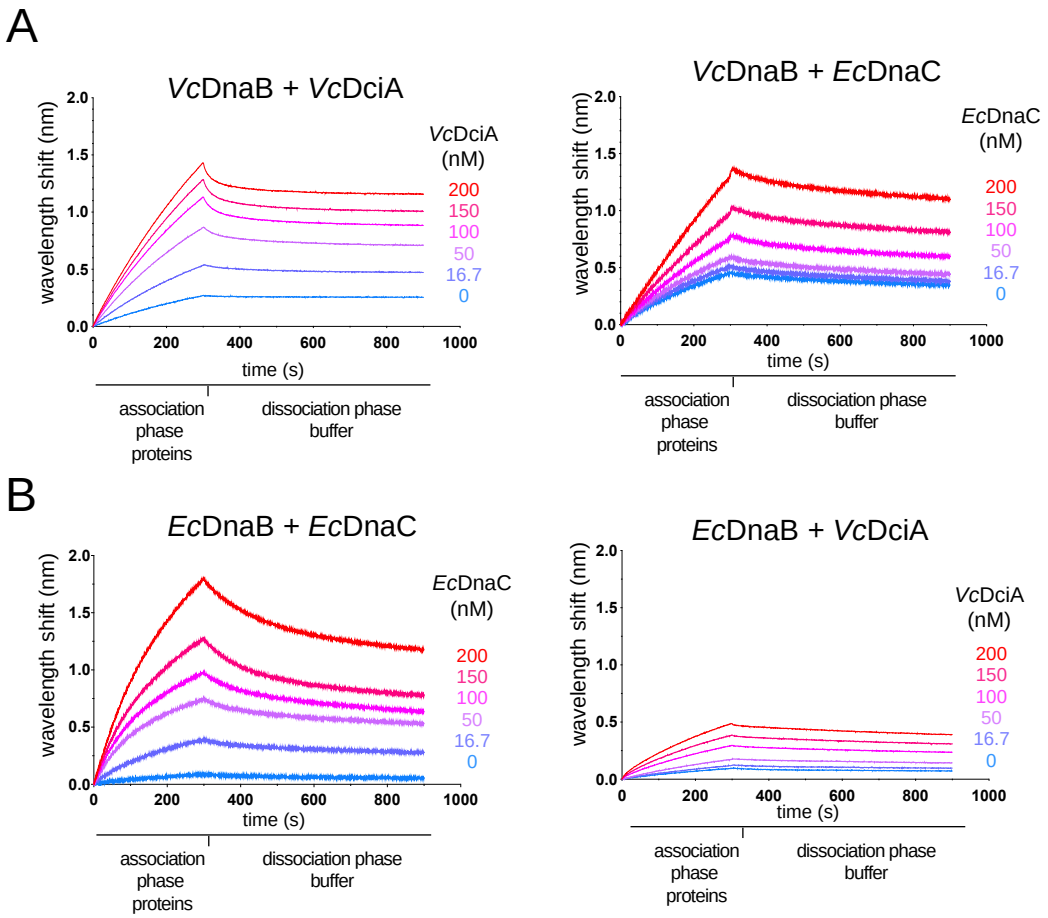
A
VcDnaB + VcDciA
wavelength shift (nm)
VcDciA (nM)
200
150
100
50
16.7
0
time (s)
association phase proteins
dissociation phase buffer
VcDnaB + EcDnaC
EcDnaC (nM)
B
EcDnaB + EcDnaC
EcDnaB + VcDciA

Fig 4

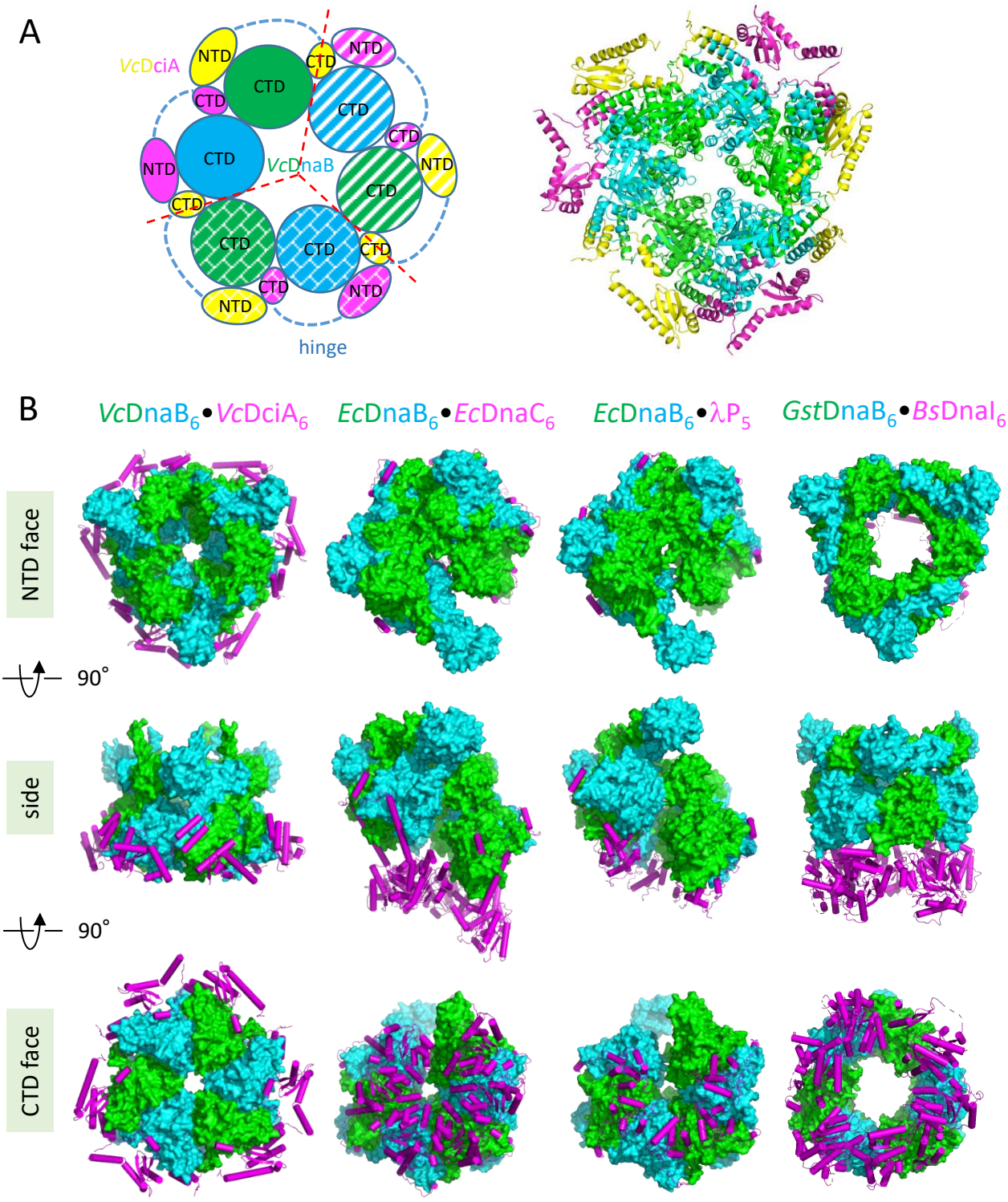
A
VcDciA
NTD
CTD
VcDnaB
hinge
B
VcDnaB6•VcDciA6
EcDnaB6•EcDnaC6
EcDnaB6•λP5
GstDnaB6•BsDnaI6
NTD face
90°
side
90°
CTD face

Supplementary Fig 1

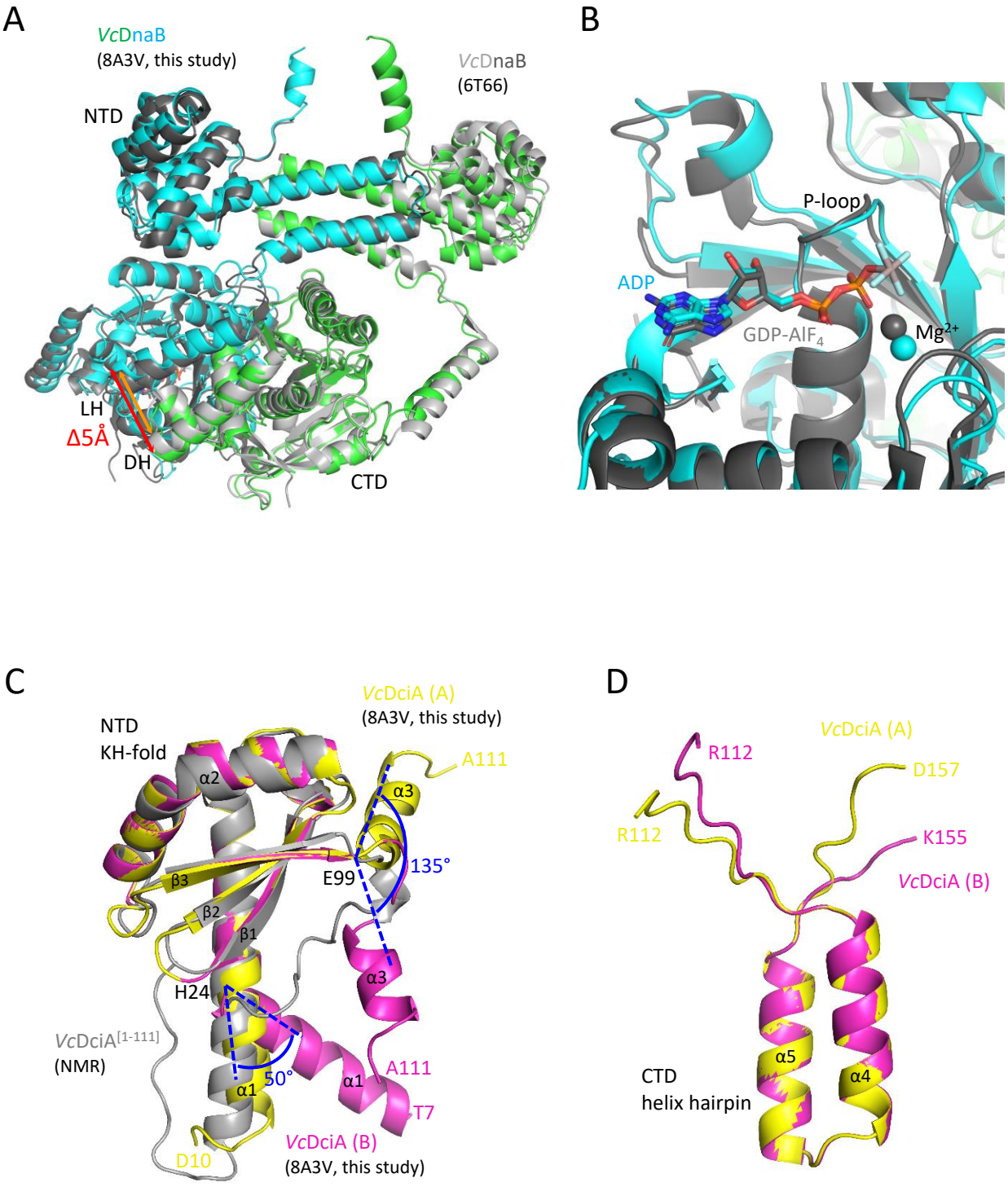

Supplementary Fig 2

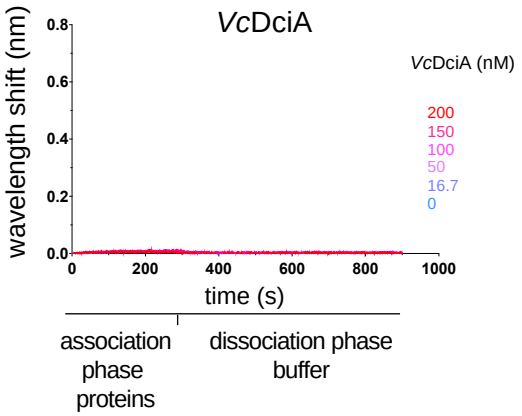

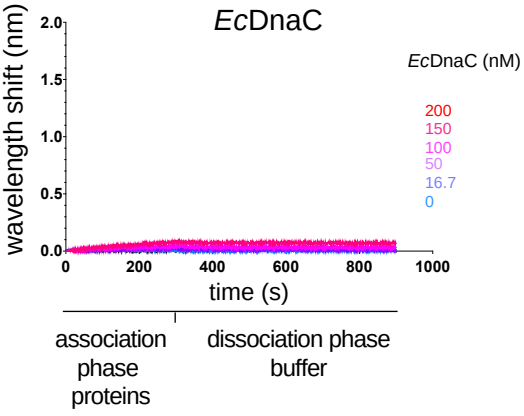

Supplementary Fig 3